Original Article

Improving Solar Photovoltaic Power System Performance Based on Maximum Power MPPT P&O-Fuzzy Using the Boost Converter

Tran Thuy Quynh[1], Chu Thi Thuy[1], Vo Quang Vinh[2], Vo Thanh Ha[3]

[1]*Department of Control and Automation, Faculty of Electrical Engineering, University of Economics-Technology for Industries, Hanoi City, Vietnam.*
[2]*Department of Control Engineering, University of Electricity, Hanoi, Vietnam.*
[3]*Department of Cybernetics, Faculty of Electrical and Electronic Engineering, University of Transport and Communications, Hanoi City, Vietnam.*

[3]*Corresponding Author : vothanhha.ktd@utc.edu.vn*

Abstract - *This paper introduces the MPPT control method to help PV solar cells reach maximum capacity thanks to the adaptive Fuzzy P&O MPPT algorithm. The power from the PV source through the traditional PI-controlled boost converter has a working point that always follows the MPPT point. Thanks to the Fuzzy P&O algorithm that allows adaptive correction of the perturbation step, the power can quickly reach a new maximum value when the ambient temperature and illuminance fluctuate. The new algorithm also eliminates oscillation around the MPPT's entire operating point and improves the output voltage quality of the boost converter. The advantage of the adaptive Fuzzy P&O MPPT algorithm is confirmed by simulation on MATLAB with a 3.5kW, 100V for a PV system.*

Keywords - *PV, MPPT-Fuzzy, Boost converter, Solar power system, MATLAB.*

1. Introduction

Today, renewable energy sources such as solar and wind power play an increasingly important role in life and industry [1-2]. In particular, solar energy has been contributing a part to the grid power of each country. Maximum Power Point Tracking (MPPT) algorithms for PV solar energy sources are becoming more and more complete and widely applied [3-6]. Among the standard MPPT algorithms, the Perturbation and Observation (P&O) algorithm is effective and widely used [7]. Many papers are still proposing new MPPT algorithms to detect MPP maximum power working points in the context of fluctuating ambient temperature and illuminance [8-10], grid-connected PV solar energy source. In addition, grid-connected PV sources with variable load and voltage [11]. The proposed MPPT algorithms are also increasingly diverse and efficient, including classic P&O and INC algorithms [12], back-propagation adaptive MPPT algorithms [13], extreme detection MPPT algorithms (extremum seeking) [14], the geometric MPPT algorithm combines sliding mode control [15], the neural algorithm [16], the slide mode algorithm [17] and many other diverse MPPT algorithms.

Recently, the research direction of combining the classic MPPT P&O and INC algorithms with sustainable adaptive control algorithms has proved very promising. Other studies propose an adaptive MPPT P&O algorithm

[18]. Zhang et al. propose an advanced MPPT P&O algorithm with an adjustable perturbation step [19]. In [20], the author introduces an improved MPPT INC algorithm with an adaptive variable perturbation step. At the same time, the intelligent MPPT algorithms exploiting the neural model [21-22], the fuzzy model, have proved very effective, maintaining the PV solar power to operate the MPPT optimally in the fluctuating environment [23-25].

From the above achievements, the paper proposes a new adaptive Fuzzy P&O MPPT algorithm that allows flexible adjustment of the perturbation correction step of the classic P&O algorithm. The new Fuzzy P&O adaptive MPPT algorithm has superior quality compared to the traditional MPPT P&O algorithm, stable operation in the entire working area of PV solar power, thoroughly eliminating fluctuations around the working point. MPP also accelerates the convergence speed to the MPP working point when the ambient temperature and illuminance fluctuate. In addition, this paper will present the boost converter model by the switching network averaging method. Improve output voltage quality with PI controller-based current controller design.

The article structure includes part 1 of the general introduction. Part 2 introduces the PV solar power source model. Section 3 presents the new adaptive Fuzzy – MPPT P&O algorithm. Section 4 gives modelling and control of the Boost converter current. Part 5 presents and analyses the

simulation and experimental results of the new Fuzzy – MPPT P&O algorithm adapted to MATLAB / Simulink with a 50-W PV system. Finally, the conclusions are presented in section 6.

2. Model of Solar Energy Source PV

The nonlinear equation of V-I characteristics of PV solar energy source, including Ns cells connected in series and N_p cells connected in parallel, has the following form:

$$V_g = -I_g R_s \left(\frac{N_s}{N_p}\right) + \left(\frac{N_s}{A}\right) . ln\left\{1 + N_s I_{ph} - \frac{N_s}{N_p I_0}\right\} \quad (1)$$

Where:

A = q/AKT
q – Electric Charge
A – Completion Factor
K – Boltzmann Constant
T – Absolute temperature

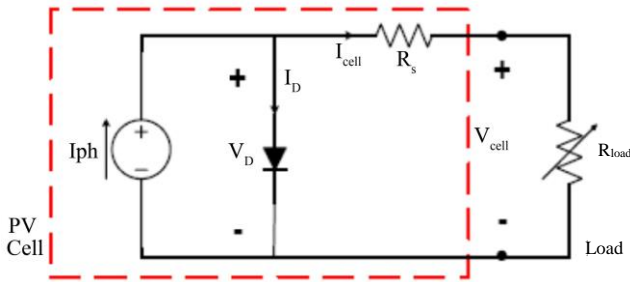The equivalent circuit of the PV solar cell is shown in Figure 1.

Fig. 1 Equivalent electricity of solar cell source PV

The *V-I* characteristic depends on the illuminance percentage Kins expressed by the expression:

$$V_g = -0.9I_g + 123,69ln\{1,0 + 123,45(13,45K_{ins} - I_g)\} \quad (2)$$

From there, we have a family of V-I standard curves according to the illuminance of PV solar cells shown in Figure 2.
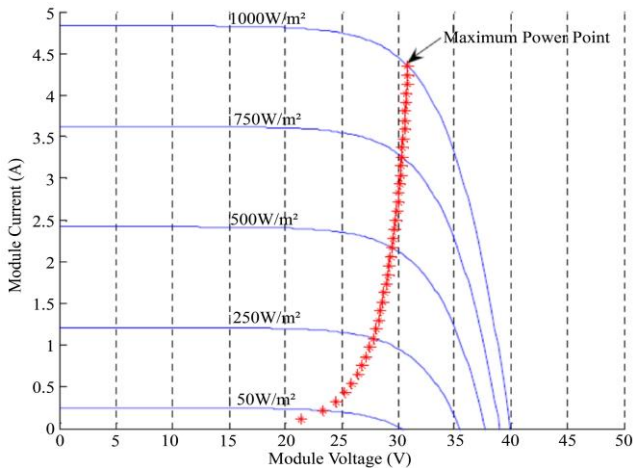

Fig. 2 Standard characteristic curve family V-I according to parameters

3. MPPT P&O Algorithm Combined with Fuzzy Logic (FL) Control

3.1. MPPT Algorithm P&O

This is the most commonly used MPPT detection algorithm based on voltage perturbation and dP/dt observations. This derivative shows whether the voltage is high or low and needs to decrease or increase until the product is zero. The principle of Maximum Power Point Tracking (MPPT) of the P&O algorithm is shown in Figure 3. The P&Q algorithm diagram is shown in Figure 4.
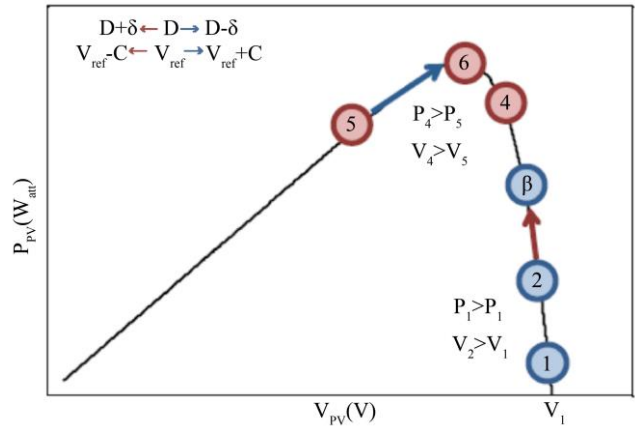

Fig. 3 Principle of Maximum Power Point Tracking (MPPT) of P&O algorithm

A summary of the operating principle of the P&O algorithm is given in Table 1:

Table 1. Principle of the P&O algorithm

Case	Noise dV	Change in Power dP	Next Noise
1	dV>0	dP>0	Positive
2	dV>0	dP<0	Minus
3	dV<0	dP>0	Minus
4	dV<0	dP<0	Positive

The 4th case of Table 1 shows that the output power is reduced by reducing the operating voltage, so the next noise step must be positive, which means the voltage needs to be increased. The detailed control diagram of the P&O algorithm is shown in Figure 5.

Figure 5 shows that at the beginning of the cycle of the P&O method, two sensors are used to measure the output current and voltage of the PV photovoltaic source. From there, calculate instantaneous power $P_n = U_n . I_n$. Then, compare the immediate power value Pn with the previous value P_{n-1}. If the power $P_n = P_{n-1}$, update the matter immediately and terminate the process. The algorithm increases voltage if the power and voltage difference between two consecutive cycles is positive. Otherwise, it decreases voltage. Conversely, if the voltage and power difference between two successive cycles is negative, the algorithm improves the voltage or decreases the operating voltage. The process is repeated until the maximum power is obtained.
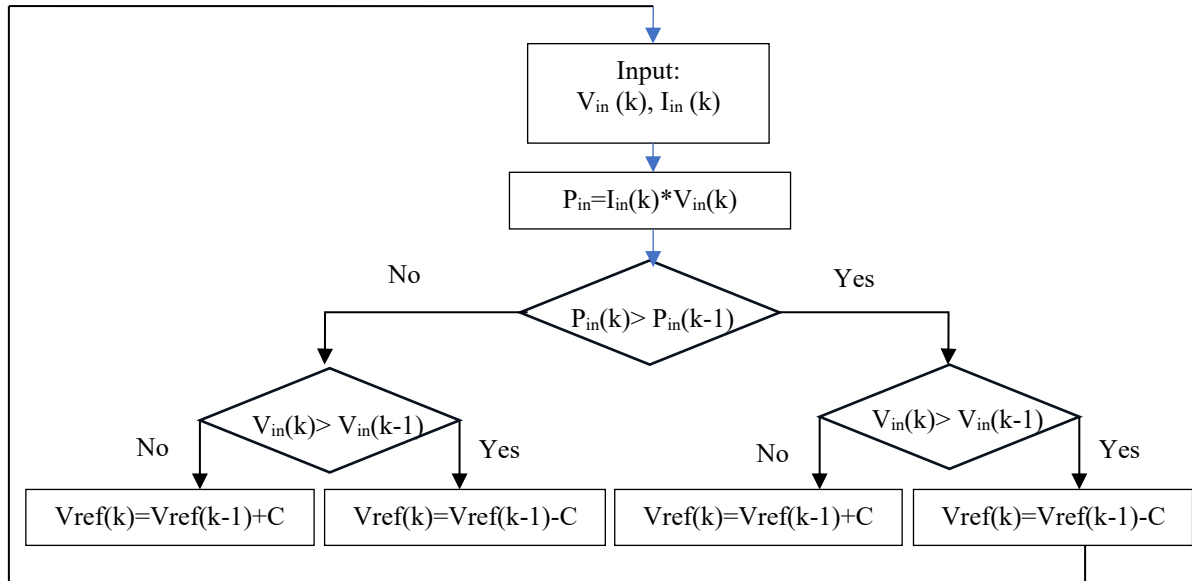
Input:
$V_{in}(k)$, $I_{in}(k)$

$P_{in}=I_{in}(k)*V_{in}(k)$

No — $P_{in}(k)>P_{in}(k-1)$ — Yes

$V_{in}(k)>V_{in}(k-1)$

No — Vref(k)=Vref(k-1)+C

Yes — Vref(k)=Vref(k-1)-C

$V_{in}(k)>V_{in}(k-1)$

No — Vref(k)=Vref(k-1)+C

Yes — Vref(k)=Vref(k-1)-C

Fig. 4 Shows the output power of PV as a function of current

Start

Do
$I_{PV}[n]$, $V_{PV}[n]$

$P_{PV}[n]=V_{PV}[n].I_{PV}[n]$
$\Delta P=P_{PV}[n]-P_{PV}[n-1]$
$\Delta V=V_{PV}[n]-V_{PV}[n-1]$

$\Delta P>0$

Yes — $V>0$

No

Yes — Voltage increase V_{PV}

No — Voltage drop V_{PV}

$\Delta V>0$

Yes — Voltage drop V_{PV}

No — Voltage increase V_{PV}

$P_{PV}[n-1]=P_{PV}[n]$
$V_{PV}[n-1]=V_{PV}[n]$
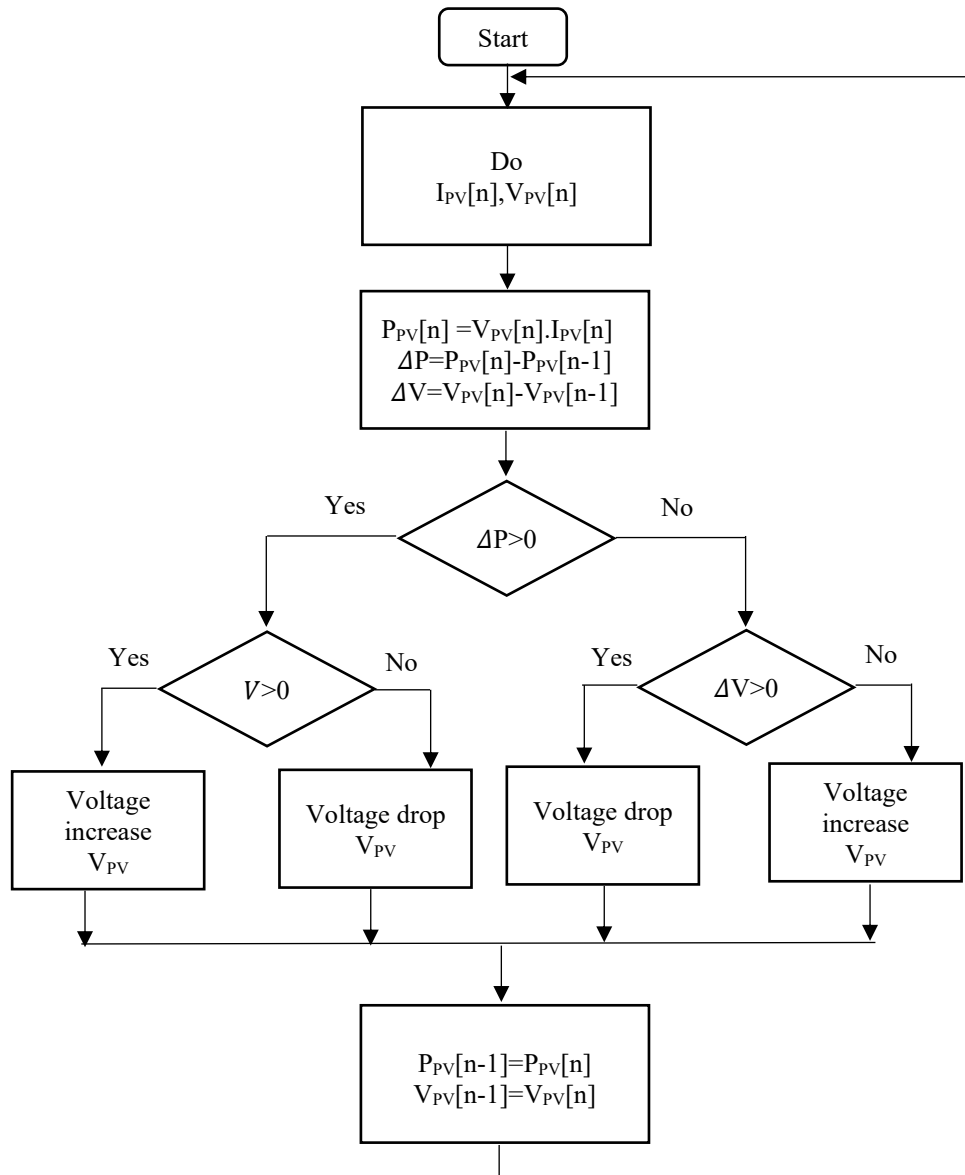
Fig. 5 Control diagram of the P&O algorithm

3.2. The Proposed Fuzzy P&O MPPT Algorithm

Fuzzy logic is one of the intelligent control methods and is being applied in many control fields today. The Fuzzy controller can receive and process complex and unstable information, correct errors and provide optimal solutions for control objects to work better. FL provides an inference method that can mimic human reasoning for application to knowledge-based systems. There are three stages in the FL control algorithm shown in Figure 6, namely, fuzzy, inference, and defuzzification methods [7] and [8].
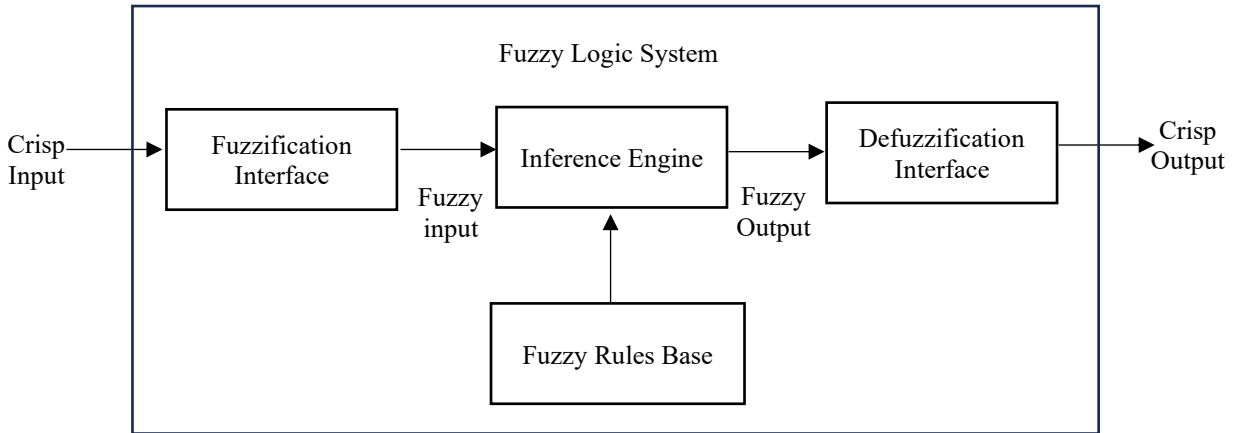
Fig. 6 Basic structure of the fuzzy controller

3.3. Fuzzification

It is making it possible to transform real variables into fuzzy variables. The actual voltage and current of the PV array can be continuously measured, and the power can be calculated. The input variables of the proposed FL controller are ΔP and ΔV. These variables are defined as follows:

There is P[k], V[k], the equivalent of the power change and voltage application of the PV array at time *k*.

The input parameter set is described by the set {NB, NM, NS, ZE, PS, PM, PB}, where NB is a large decrease, NM is an average decrease, NS is a small decrease, ZE is no increase, no decrease, PS is a small increase, PM is a medium increase, and PB is a large increase. The fuzzy set value is shown in Figure 6.
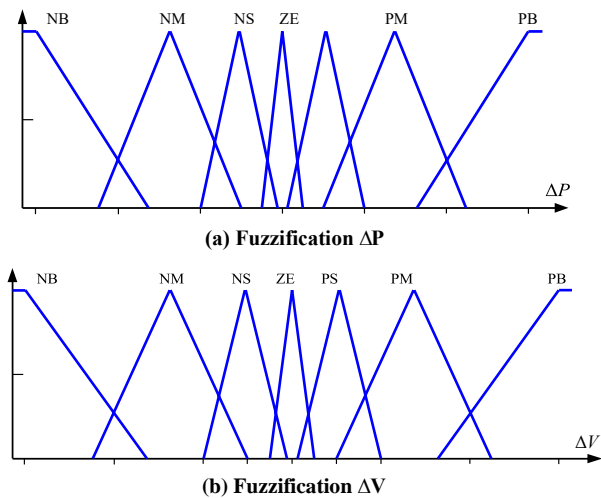

(a) Fuzzification ΔP

(b) Fuzzification ΔV
Fig. 7 Fuzzification value of 2 inputs

3.4. Inferential Methods

$$\Delta P = P[k] - P[k-1] \qquad (3)$$

$$\Delta V = V[k] - V[k-1] \qquad (4)$$

Since *V* out is kept constant, V_{in} will be inversely proportional to pulse width *d*.

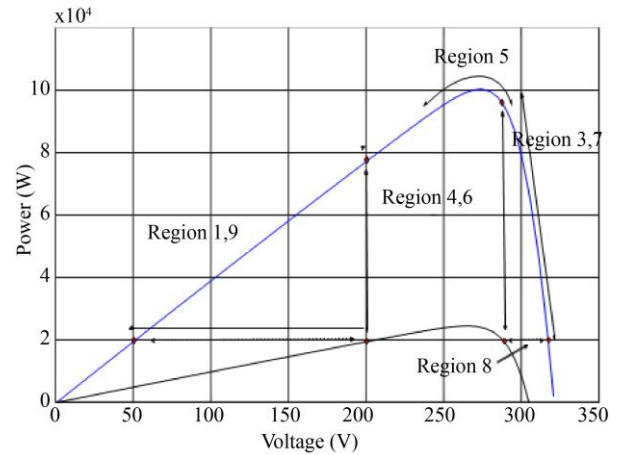Figure 8, fuzzy control rules can be deduced. The characteristics of the panel are divided into 9 zones [8].

Fig. 8 Characteristic line P – V of the array PV

Based on the relationship between voltage error and power command error, a fuzzy set of input and output values, the fuzzy controller is designed based on the control rule system defined as shown in Figure 4 [8].

Table 1. Fuzzy rules

Fuzzy Rules		ΔP						
		NB	NM	NS	ZE	PS	PM	PB
ΔV	NB	NB	NB	NB	ZE	PB	PB	PB
	NM	NB	NB	NM	ZE	PM	PB	PB
	NS	NB	NM	NS	ZE	ZE	PB	PB
	ZE	ZE	ZE	ZE	ZE	ZE	ZE	ZE
	PS	PB	PM	PM	ZE	NS	NM	NB
	PM	PB	BP	PM	ZE	NM	NM	NB
	PB	PB	PB	PB	ZE	NB	NB	NB

3.5. Defuzzification

The set of output parameters is described by the group {NB, NM, NS, ZE, PS, PM, PB}, where NB is a significant decrease, NM is a medium decrease, NS is a slight decrease,

ZE has no increase and no decrease, PS has a slight increase, PM has a medium increase, and PB has a significant increase. The value of the fuzzy set is shown in Figure 9.
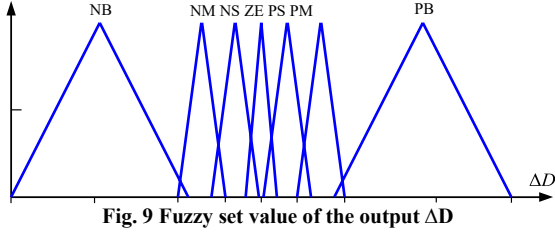

Fig. 9 Fuzzy set value of the output ΔD

4. Boost Converters

4.1. Modelling the Boost Variable with the Closed Network Average Method

The method of averaging the switching network is of interest today because the obtained model is close to the physical model, which can describe the loss-causing elements such as resistance when conducting current through the valve, voltage drop on valves, and some parasitic electrical circuits.

The purpose of the method is to replace the part of the circuit with the switching element with a two-door network. Then, the nonlinear switching network is replaced with a linear network through averaging.

On the diagram boost converter Figure 10, the switching network includes valve MOSFET and diode. Because the input current to port 1 $i_1(t)$ is the current through the inductor, it can be considered an independent variable; the output voltage on the capacitor $v_2(t)$ is the voltage on the load that changes only when the load changes, so also consider is the independent variable. Therefore, voltage $v_1(t)$ and $i_2(t)$ are considered dependent variables, as shown in Figure 11.
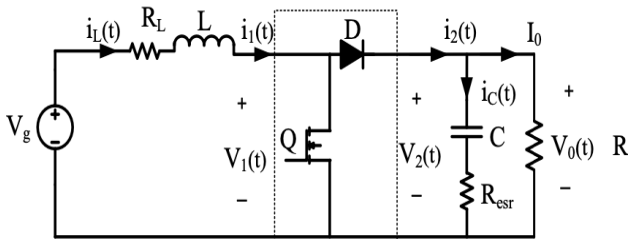

Fig. 10 The switching circuit in the diagram boosts the converter

Their waveforms are shown in Figure 8 according to the operation analysis of the Boost converter diagram. Average voltage $v_1(t)$ and current $i_2(t)$ over a period T_s assuming $v_2(t)$ and $i1(t)$ pulses are negligible or vary almost linearly:

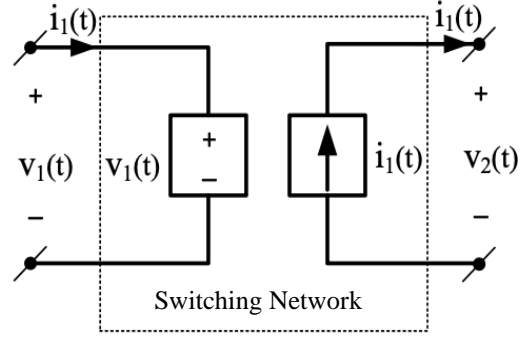$$(V_1(t))_{T_s} = (1 - d(t))(V_2(t))_{T_s} = d'(t)(V_2(t))_{T_s} \quad (5)$$

Fig. 11 Switched network model

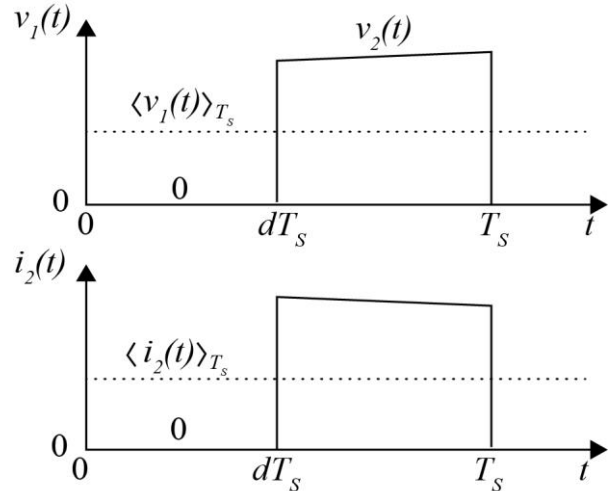$$(i_1(t))_{T_s} = (1 - d(t))(i_1(t))_{T_s} = d'(t)(i_2(t))_{T_s} \quad (6)$$

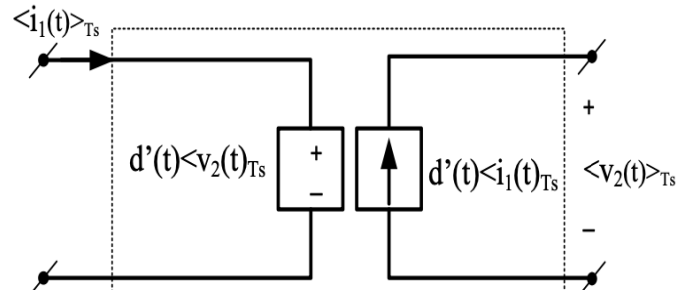**Fig. 12 Voltage form V1(t) on MOSFET and current form $i_2(t)$ through diode**

Fig. 13 Average model

Proceed to linearize the model in Figure 9 by introducing small fluctuations:

$$\begin{pmatrix} V_g(t) = V_g + \widehat{V_g}(t) \\ i_L(t) = I_L + \widehat{i_L(t)} \\ V_1(t) = V_1 + \widehat{V_1(t)} \\ i_2(t) = I_2 + \widehat{i_2}(t) \\ V_2(t) = V_2 + \widehat{V_2(t)} \\ d = D' + \widehat{d(t)} \\ d' = 1 - d = D' + \widehat{d(t)} \end{pmatrix} \quad (7)$$

The dependent voltage source at input port 1 becomes:

$$\langle V_1(t)\rangle = d'(t)\langle V_2(t)\rangle = \left(D' - \hat{d}(t)\right)\left(V_2 + \widehat{V_2}(t)\right)$$
$$\approx D'\left(V_2 + \widehat{V_2}(t)\right) - V_2\hat{d}(t) \qquad (8)$$

First term $D'\left(V_2 + \widehat{V_2}(t)\right)$ shows the dependence on the output voltage $\left(V_2 + \widehat{V_2}(t)\right)$ in proportion D', described by the dependent voltage source. Rank $V_2\hat{d}(t)$ is the source controlled by the modulation factor $\hat{d}(t)$ and should become an independent voltage source connected in series in the circuit. The dependent current is shown:

$$\langle i_2(t)\rangle = d'(t)\langle i_1(t)\rangle = \left(D' - \hat{d}(t)\right)\left(I_1 + \widehat{I_1}(t)\right)$$
$$\approx D'\left(I_1 + \widehat{i_1}(t)\right) - I_1\hat{d}(t) \qquad (9)$$

Rank $D'\left(I_1 + \widehat{i_1}(t)\right)$ express dependence on $\left(I_1 + \widehat{i_1}(t)\right)$ in proportion D' should be described by the dependent current source. Rank $I_1\hat{d}(t)$ is the current source controlled by the factor $\hat{d}(t)$ and becomes an independent current source in parallel with the circuit. From there, the average model of the switching network for the boost circuit.
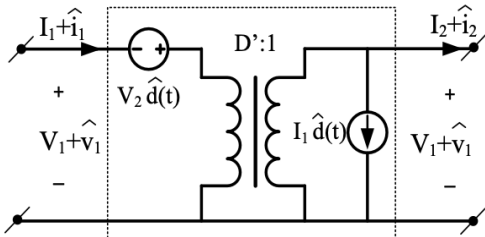

Fig. 14 Switching network average model for boost converter

From the above analysis, the average model for the Boost converter is shown:
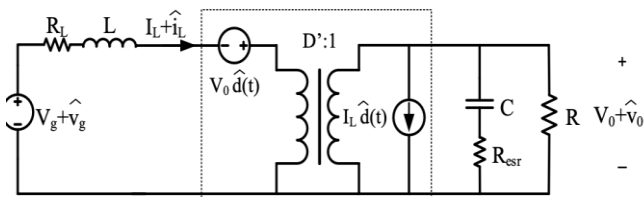

Fig. 15 Average model for boost circuit

Considering the small signal model, as shown in Figure 15, it is necessary to determine the important transfer functions for the design of the current controller:

$$\begin{cases} G_{VD} = \dfrac{\widehat{v_0}}{\hat{d}}\bigg|_{\widehat{v_g}=0} \\[2mm] G_{id} = \dfrac{\widehat{i_L}}{\hat{d}}\bigg|_{\widehat{v_g}=0} \end{cases} \qquad (10)$$

To find these transfer functions, we remove the influence of the source $\widehat{v_g} = 0$ in the model Figure 16&17 to obtain a simple model:
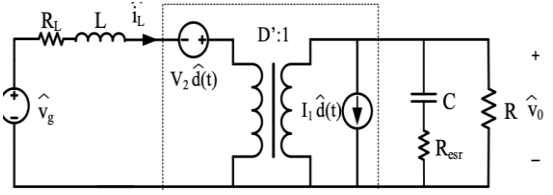

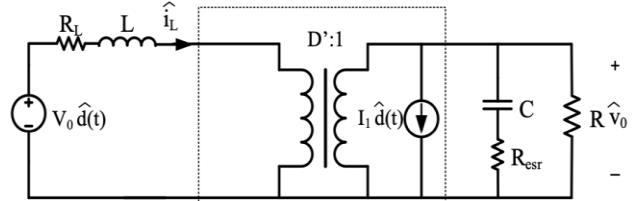**Fig. 16 Small signal average model for boost circuit**

Fig. 17 Small signal average model for boost circuit when $\widehat{v_g} = 0$

Next, convert to the transformer's primary, Laplace the circuit, and then, based on the circuit calculation, derive the desired transfer function G_{vd} and G_{id}.
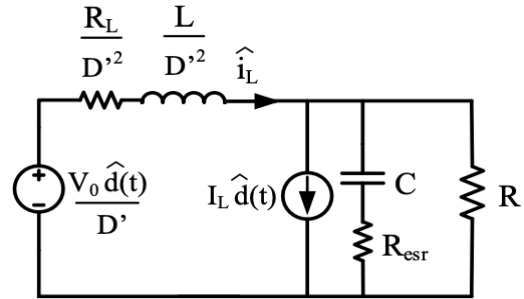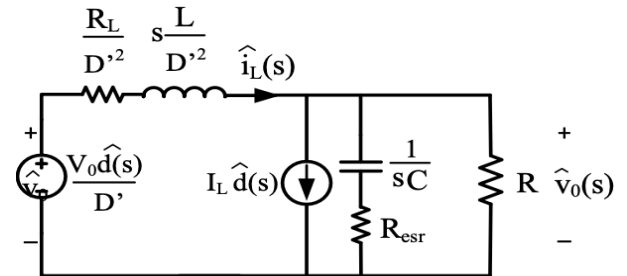

Fig. 18 The secondary conversion models

Fig. 19 Laplace of the converter circuit

The voltage balance in the circuit shown in Figure 19 is obtained:

$$G_{vd}(s) = \frac{\widehat{V_0}(s)}{\hat{d}(s)}$$
$$= \frac{V_0}{D'}\frac{\left(1 - \dfrac{R_L + sL}{RD'^2}\right)(1 + sR_{esr}C)}{s^2\dfrac{LC(R + R_{esr})}{RD'^2} + s\left(\dfrac{R_L(R + R_{esr})C + L}{RD'^2} + R_{esr}C\right) + \dfrac{R_L}{RD'^2} + 1} \qquad (11)$$

The current balance in the circuit shown in Figure 15 is obtained:

$$\hat{i}_L(s) = \frac{1}{D'}\left[I_L\hat{d}(s) + \frac{s(R+R_{esr})C+1}{(1+sR_{esr}C)R}\hat{v}_0(s)\right] \qquad (12)$$

Combined with $\hat{v}_0 t$ from the transfer function, the transfer function of the current object can be deduced:

$$G_{id}(s) = \frac{\hat{\imath_L}(s)}{\hat{d}(s)} =$$

$$\frac{\frac{V_0}{RD'^2}\,\frac{s(R+2R_{esr})C+2}{s^2\frac{LC(R+R_{esr})}{RD'^2}+s\left(\frac{R_L(R+R_{esr})C+L}{RD'^2}+R_{esr}C\right)}}{+\frac{R_L}{RD'^2}+1}$$ (13)

4.2. Design of Current Controller

The diagram of the control current is shown in Figure 20. The current control loop has fast dynamic characteristics, and the voltage loop has lower dynamic features. As a result, the inductor current can vary very quickly compared to the output voltage.

According to Equation (13), the transfer function of the current control loop:

$$G\_id(s)=(0,008347s+48)/(1,739.⟦10⟧^{(-8)}.s^2+7,658.⟦10⟧^{(-5)}\,s+4,07)$$ (14)
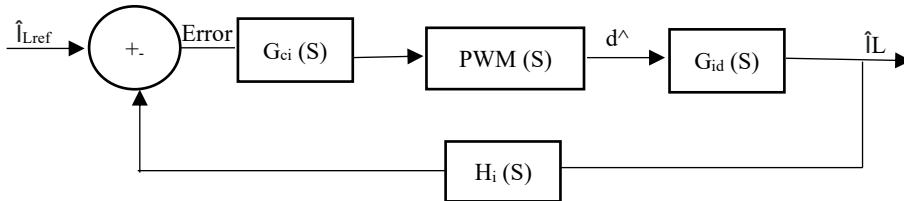

Fig. 20 The diagram of the control current

5. Results and Discussion

The MATLAB simulations of a structure fuzzy logic-based MPPT controller and a boost converter are built, as shown in Figure 21. The surface view of the FL model is expressed in Figure 22. The fuzzy rules for two inputs and output are shown in Figure 23. Power rating input from the user = 2.00 kW. Minimum number of panels required per string = 8. Maximum number of panels connected per string without reaching maximum voltage = 10. The minimum power rating of the solar PV plant = 1.80 kW. Maximum power possible per string without reaching maximum DC voltage = 2.25 kW. Actual number of panels per string = 9. Number of strings connected in parallel = 1. Actual solar PV plant power = 2.03 kW.
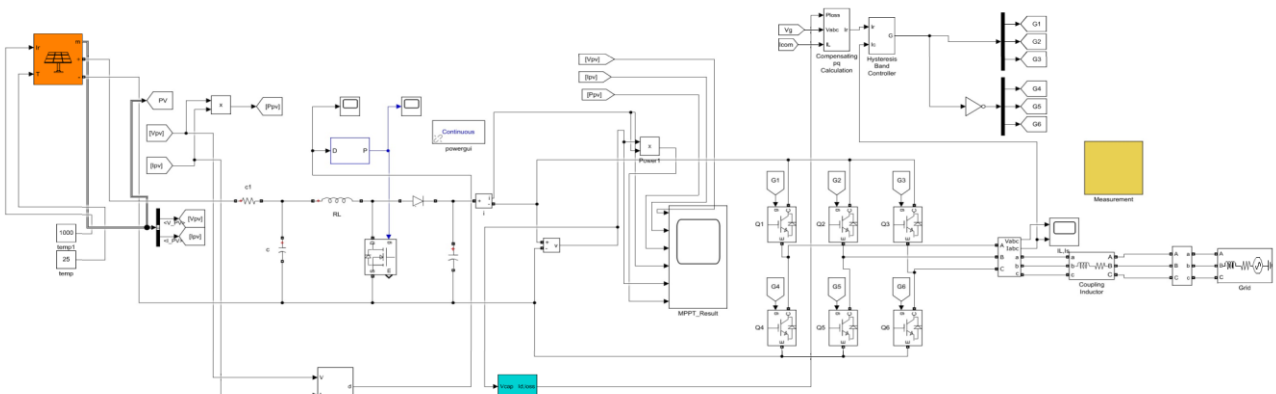

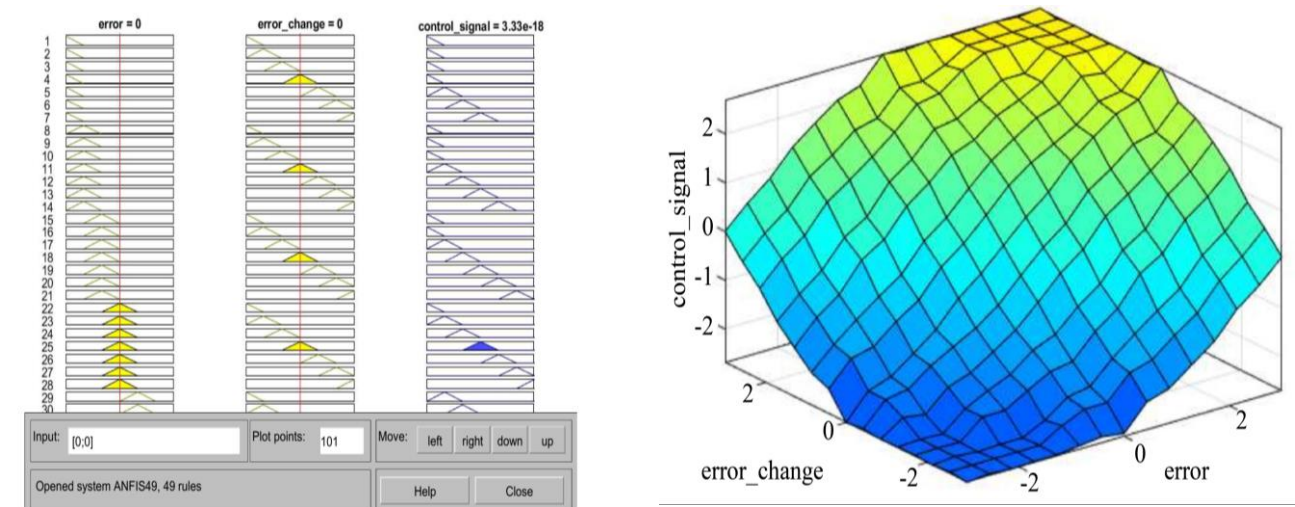**Fig. 21 The structure of FL based MPPT controller and a boost converter**

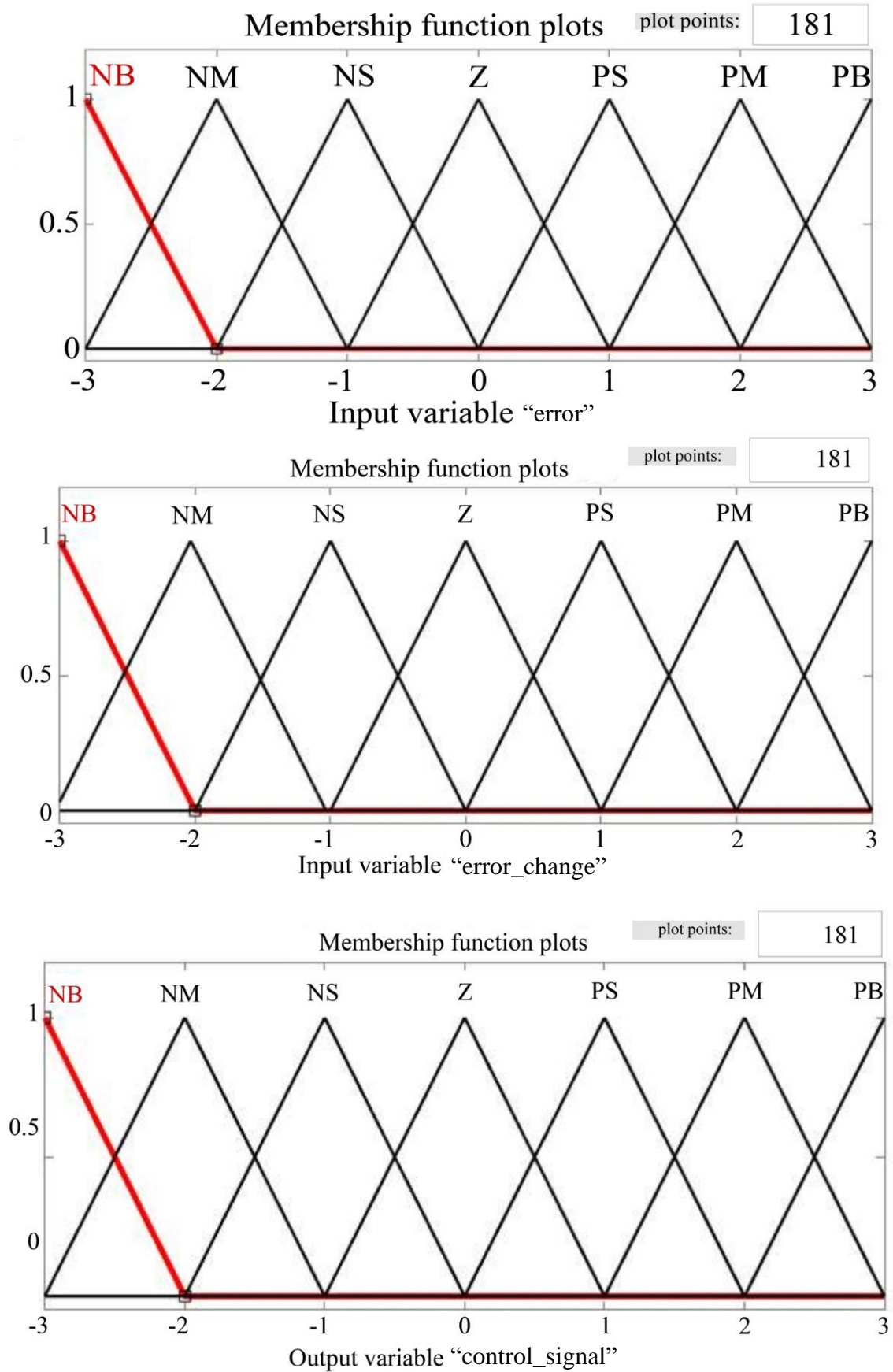**Fig. 22 The surface view of the FL model**

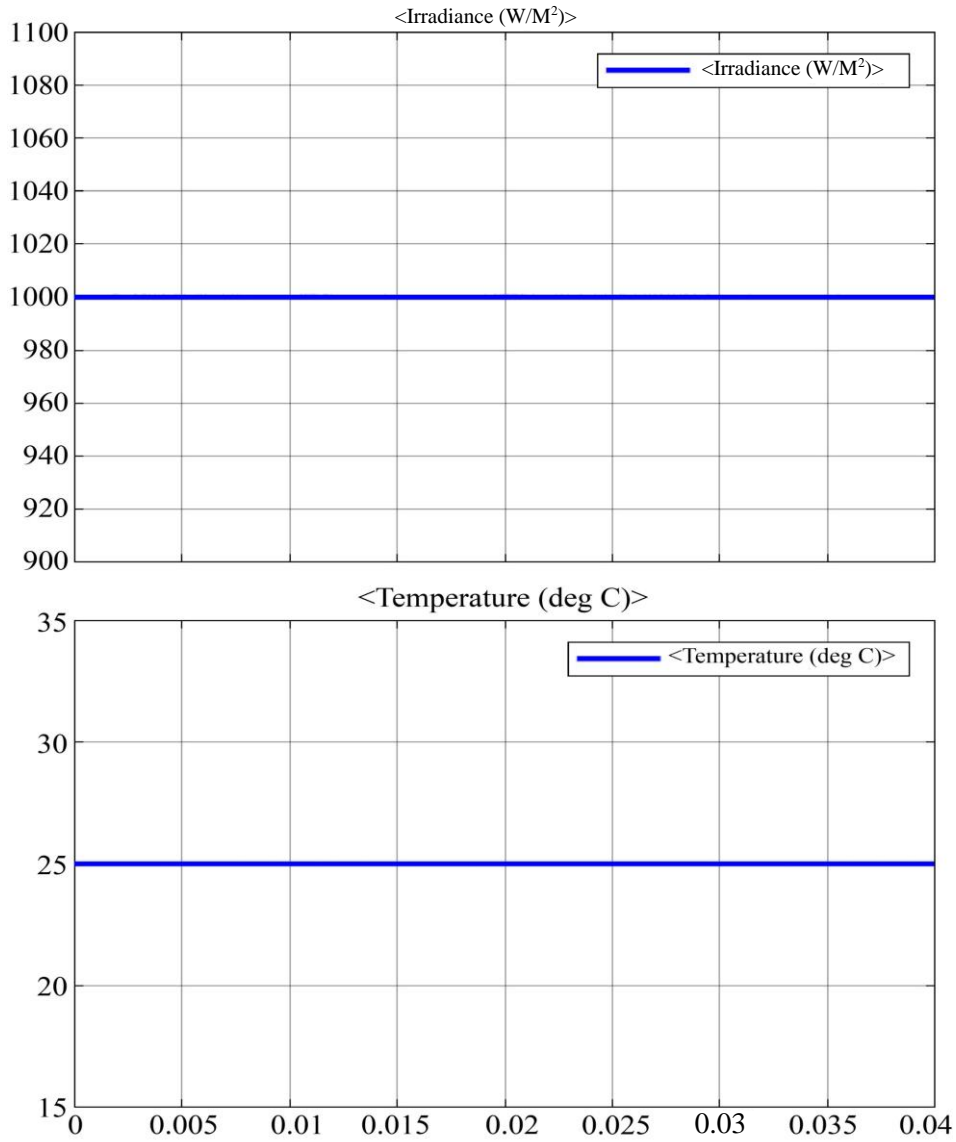Fig. 23 The fuzzy rule for two inputs and an output

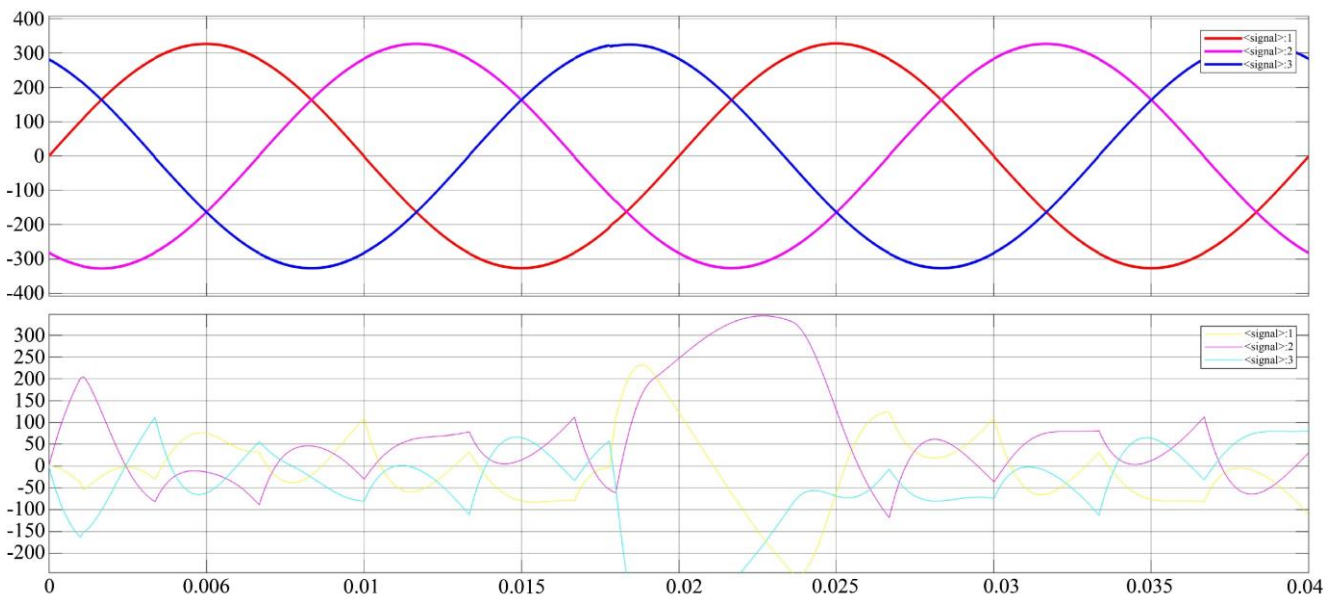**Fig. 24 Irradiance is 1000 W/m², and the temperature kept constant at 25°C**

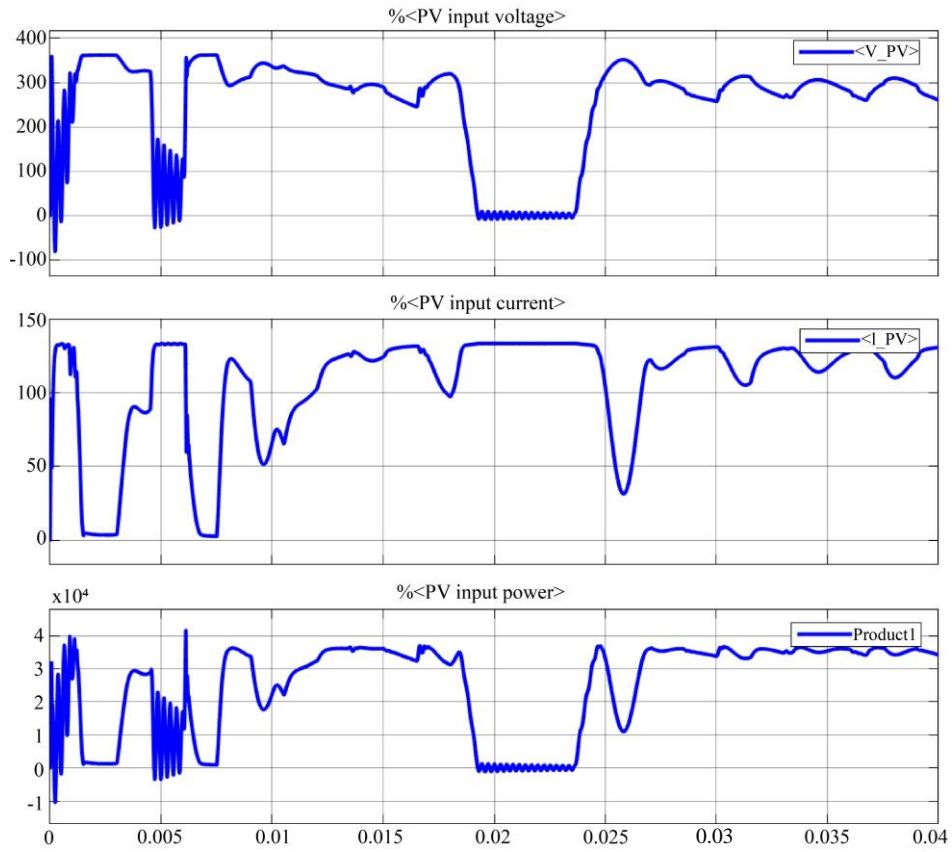**Fig. 25 Three phases' currents**

Fig. 26 The input voltage, current, and power for PV system
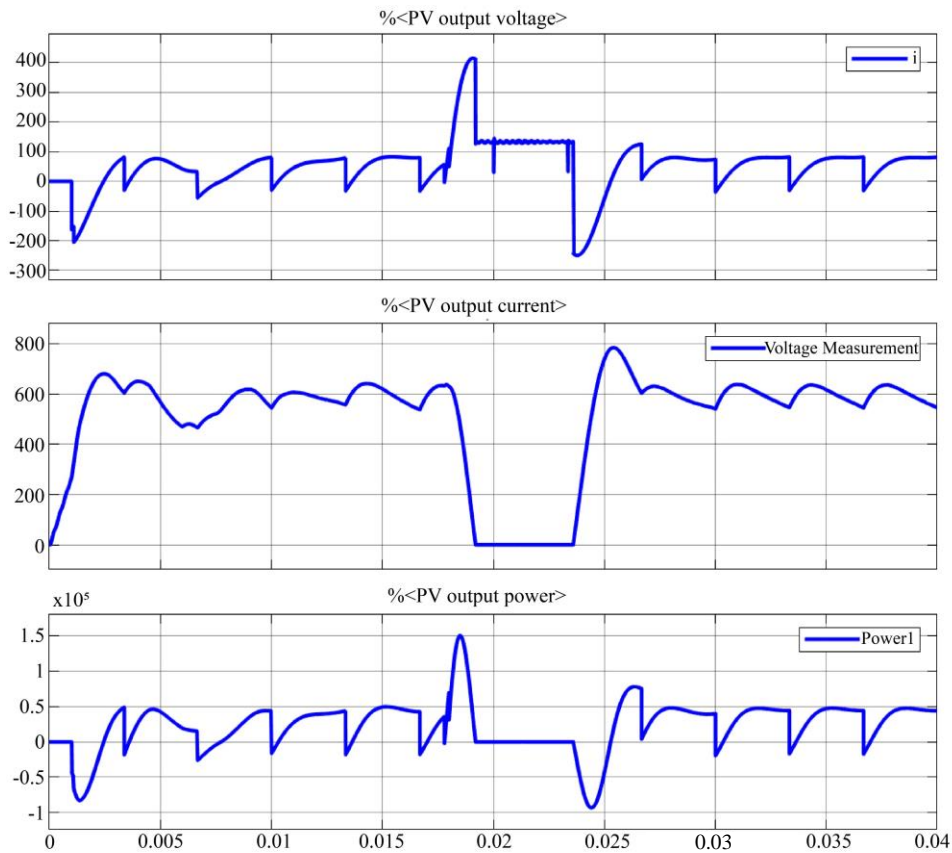

Fig. 27 The output voltage, current, and power for PV system

The selected parameters of the boost converter are shown in Table 2.

Table 2. Selected parameters of the boost converter

Parameter	Value
Input voltage	98V
Input current	140A
Duty ratio	0.35
Inductor	4mH
Load resistance	12 Ω
Output capacitor	89µF
Input capacitor	4500 µF
Switching frequency	20kHz

Irradiance is 1000 W/m2, and the temperature kept constant at 25°C is shown in Figure 25. Three phases' currents are shown in Figure 24. The output voltage, current, and power for the PV system are shown in Figure 26.

Based on the above simulation results (Figures 24, 25, 26, and 27), the proposed MPPT controller is simulated at STC (1000 W/m2 and 25 °C). The PV power output rises sharply from zero up to about the FL- MPPT P&O (500 W) after a time of 10 ms. For the system with the FL- MPPT P&O controller, the power output settles at MPP since the MPPT controller will continuously force the PV module to operate at the FL- MPPT P&O. For the system without the controller, the PV power input drops and settles at around 3,5kW. The PV input current is about 140A, and the input voltage is about 350V. Meanwhile, the PV power output for the boost converter drops at approximately 500W. This is because the load resistance does not match the internal resistance of the module. In addition, the sine three-phase current and the PV input current are about 600A, and the input voltage is about 100V. This proves that the FL-MPPT P&O controller works well and efficiently.

6. Conclusion

The ability to extract more energy from a given quantity of solar radiation is made feasible by incorporating FL-MPPT P&O peak power scoring algorithms into Boost converters. The MATLAB/Simulink simulation results in this paper's simulation show that both the -MPPT P&OFL algorithms can identify the most effective max power point. The acquired data also demonstrate that the algorithms' performance and reaction times would vary depending on the weather. The collected study findings confirm that the suggested FL control algorithm with MPPT consistently achieves high performance under fluctuating radiation circumstances and is the best algorithm among those examined. The study findings will be applied to actual devices in the future and further contrasted with other control techniques to show the solution's efficacy.

Acknowledgements

References

[1] H.A. Walker, Jal Desai, and D.M. Heimiller, *Performance of Photovoltaic Systems Recorded by Open Solar Performance and Reliability Clearinghouse (oSPARC)*, No. NREL/TP-5C00-75162, National Renewable Energy Lab, pp. 1-28, 2020. [CrossRef] [Google Scholar] [Publisher link]

[2] Dolf Gielen et al., *Global Renewables Outlook: Energy Transformation 2050*, International Renewable Energy Agency IRENA, pp. 1-212, 2020. [Google Scholar] [Publisher link]

[3] Maria Van Der Hoeven, *Technology Roadmap Solar Photovoltaic Energy*, OECD/IEA, pp. 1-44, 2010. [Google Scholar] [Publisher link]

[4] Adel Mellit, and Soteris A. Kalogirou, "MPPT-Based Artificial Intelligence Techniques for Photovoltaic Systems and its Implementation into Field Programmable Gate Array Chips: Review of Current Status and Future Perspectives," *Energy*, vol. 70, pp. 1-21, 2014. [CrossRef] [Google Scholar] [Publisher link]

[5] Amalraj Peter Amalathas, and Maan M. Alkaisi, "Nanostructures for Light Trapping in Thin Film Solar Cells," *Micromachines*, vol. 10, no. 9, pp. 1-18, 2019. [CrossRef] [Google Scholar] [Publisher link]

[6] D.F. Teshome, "A Modified Firefly Algorithm for Photovoltaic Maximum Power Point Tracking Control under Partial Shading," *IEEE Journal of Emerging and Selected Topics in Power Electronics*, vol. 5, no. 2, pp. 661-671, 2017. [CrossRef] [Google Scholar] [Publisher link]

[7] Cherukuri Santhan Kumar, and Rayapudi Srinivasa Rao, "A Novel Global MPP Tracking of Photovoltaic System Based on Whale Optimization Algorithm," *International Journal of Renewable Energy Development*, vol. 5, no. 3, pp. 225-232, 2016. [CrossRef] [Google Scholar] [Publisher link]

[8] Al-Attar Ali Mohamed, Ahmed Lotfy Haridy, and A.M. Hemeida, "The Whale Optimization Algorithm Based Controller for PMSG Wind Energy Generation System," *2019 International Conference on Innovative Trends in Computer Engineering (ITCE)*, pp. 438-443, 2019. [CrossRef] [Google Scholar] [Publisher link]

[9] Kok Soon Tey et al., "Improved Differential Evolution-Based MPPT Algorithm Using SEPIC for PV Systems under Partial Shading Conditions and Load Variation," *IEEE Transactions on Industrial Informatics*, vol. 14, no. 10, pp. 4322-4333, 2018. [CrossRef] [Google Scholar] [Publisher link]

[10] Ke Guo et al., "An Improved Gray Wolf Optimizer MPPT Algorithm for PV System with BFBIC Converter under Partial Shading," *IEEE Access*, vol. 8, pp. 103476-103490, 2020. [CrossRef] [Google Scholar] [Publisher link]

[11] Bhubaneswari Parida, S. Iniyan, and Ranko Goic, "A Review of Solar Photovoltaic Technologies," *Renewable and Sustainable Energy Reviews*, vol. 15, no. 3, pp. 1625-1636, 2011. [CrossRef] [Google Scholar] [Publisher link]

[12] Trishan Esram, and Patrick L. Chapman, "Comparison of Photovoltaic Array Maximum Power Point Tracking Techniques," *IEEE Transactions on Energy Conversion*, vol. 22, no. 2, pp. 439-449, 2007. [CrossRef] [Google Scholar] [Publisher link]

[13] V. Salas et al., "Review of the Maximum Power Point Tracking Algorithms for Stand-Alone Photovoltaic Systems," *Solar Energy Materials and Solar Cells*, vol. 90, no. 11, pp. 1555-1578, 2006. [CrossRef] [Google Scholar] [Publisher link]

[14] Nicola Femia et al., *Power Electronics and Control Techniques for Maximum Energy Harvesting in Photovoltaic Systems,* CRC Press, pp. 1-366, 2012. [Google Scholar] [Publisher link]

[15] D.P. Hohm, and M.E. Ropp, "Comparative Study of Maximum Power Point Tracking Algorithms," *Progress in Photovoltaics: Research and Applications*, vol. 11, no. 1, pp. 47-62, 2003. [CrossRef] [Google Scholar] [Publisher link]

[16] Dezso Sera et al., "On the Perturb-and-Observe and Incremental Conductance MPPT Methods for PV Systems," *IEEE Journal of Photovoltaics*, vol. 3, no. 3, pp. 1070-1078, 2013. [CrossRef] [Google Scholar] [Publisher link]

[17] B. Bendib et al., "An Intelligent MPPT Approach Based on Neural-Network Voltage Estimator and Fuzzy Controller, Applied to a Stand-Alone PV System," *2014 IEEE 23rd International Symposium on Industrial Electronics (ISIE)*, pp. 404-409, 2014. [CrossRef] [Google Scholar] [Publisher link]

[18] Jaw-Kuen Shiau, Yu-Chen Wei, and Bo-Chih Chen, "A Study on the Fuzzy- Logic-Based Solar Power MPPT Algorithms Using Different Fuzzy Input Variables," *Algorithms*, vol. 8, no. 2, pp. 100-127, 2015. [CrossRef] [Google Scholar] [Publisher link]

[19] Binh Nam Nguyen et al., "Propose a MPPT Algorithm Based on Thevenin Equivalent Circuit for Improving Photovoltaic System Operation," *Frontiers in Energy Research*, vol. 8, pp. 1-14, 2020. [CrossRef] [Google Scholar] [Publisher link]

[20] Binh Nam Nguyen et al., "A New Maximum Power Point Tracking Algorithm for the Photovoltaic Power System," *2019 International Conference on System Science and Engineering (ICSSE)*, pp. 159-163, 2019. [CrossRef] [Google Scholar] [Publisher link]

[21] Roberto F. Coelho, Filipe M. Concer, and Denizar C. Martins, "Analytical and Experimental Analysis of DC-DC Converters in Photovoltaic Maximum Power Point Tracking Applications," *IECON 2010 - 36th Annual Conference on IEEE Industrial Electronics Society*, pp. 2778-2783, 2010. [CrossRef] [Google Scholar] [Publisher link]

[22] Roberto F. Coelho, Walbermark M. dos Santos, and Denizar C. Martins, "Influence of Power Converters on PV Maximum Power Point Tracking Efficiency," *2012 10th IEEE/IAS International Conference on Industry Applications*, pp. 1-8, 2012. [CrossRef] [Google Scholar] [Publisher link]

[23] Robert W. Erickson, and Dragan Maksimovic, *Fundamentals of Power Electronics*, Springer US, pp. 1-883, 2001. [Google Scholar] [Publisher link]

[24] Colonel Wm. T. McLyman, *Transformer and Inductor Design Handbook*, 3rd ed., CRC Press, pp. 1-556, 2004. [CrossRef] [Google Scholar] [Publisher link]

[25] Rick Zaitsu, "Voltage Mode Boost Converter Small Signal Control Loop Analysis Using the TPS61030," *Texas Instruments*, pp. 1-21, 2009. [Google Scholar] [Publisher link]